Revista de la Facultad de Ciencias Universidad Nacional de Colombia, Sede Medellín
V 15 N°1 enero - junio 2026 • ISSN-e 2357-5749 • Research paper • Pages 111 to 129
DOI: https://10.15446/rev.fac.cienc.v15n1.119517

ENTROPY PRODUCTION DRIVES OSCILLATIONS IN AN ELECTROCHEMICAL REACTION MODEL[a]

LA PRODUCCIÓN DE ENTROPÍA CONDUCE LAS OSCILACIONES EN UN MODELO DE REACCIÓN ELECTROQUÍMICA

DANIEL BARRAGÁN[b*], CAROLINA CÁCERES-MOLANO[c],

Received 23-03-2025, accepted 23-09-2025, final version 15-12-2025.
Research paper

ABSTRACT: In this article, we present a second-law thermodynamic analysis of an electrochemical model that describes the electrooxidation of an organic substance, such as formic acid. The primary objective is to compare the entropy production rates of reactions and transport processes–heat and charge–under steady-state and sustained oscillation regimes. To conduct this study, we adjust model parameters, such as the equilibrium electrochemical potentials. One operating parameter of the electrochemical circuit acts as a dynamic bifurcation parameter; under galvanostatic conditions, the applied external current shifts the working electrode potential from a steady state to a sustained oscillatory regime, passing through a damped oscillatory phase. Our results indicate that entropy generation characterizes the dynamic regimes of chemical reactions and transport processes that emerge when the electrochemical model is operated. Notably, the average value of this second-law thermodynamic quantity is consistently higher during sustained oscillation states. This study enables further investigation into the energy efficiency of fuel cells that utilize small organic molecules, such as formic acid or methanol.

KEYWORDS: Electrooxidation; Oscillations; Entropy production.

RESUMEN: En este artículo, presentamos el análisis termodinámico de la Segunda Ley de un modelo electroquímico que describe la electrooxidación de una sustancia orgánica, como el ácido fórmico. El objetivo principal es comparar la velocidad de producción de entropía de las reacciones químicas y de los procesos de transporte, de calor y de carga, tanto en regímenes de estado estacionario como en oscilaciones sostenidas; para lograrlo, ajustamos los valores de un conjunto de parámetros del modelo, como los potenciales electroquímicos de equilibrio. Un parámetro de operación del circuito electroquímico actúa como parámetro dinámico de bifurcación; bajo condiciones de operación galvanostática, la corriente externa aplicada mueve el potencial del electrodo de trabajo de una dinámica estacionaria a una de oscilaciones sostenidas, pasando por un régimen de oscilaciones amortiguadas. Los resultados obtenidos muestran que la generación de entropía caracteriza los diferentes regímenes de las reacciones químicas y de los procesos de transporte observados durante la operación del modelo electroquímico, en los que el valor promedio de esta cantidad termodinámica de la Segunda Ley es siempre mayor en los estados de oscilaciones sostenidas. Será interesante, en un

[a]Barragán, Daniel & Cáceres-Molano, Carolina (2026). Entropy production drives oscillations in an electrochemical reaction model. *Rev. Fac. Cienc.*, 15 (**1**), 111-129. DOI: https://10.15446/rev.fac.cienc.v15n1.119517

[b]Departamento de Química. Facultad de Ciencias. Universidad Nacional de Colombia-Sede Medellín.
[*]Corresponding author: dalbarraganr@unal.edu.co
[c]Semillero FILOSOFÍA Y EDUCACIÓN DE LA CIENCIA. Facultad de Ciencias. Universidad Nacional de Colombia-Sede Medellín.

futuro próximo, profundizar en este tipo de estudios con el propósito de analizar la eficiencia energética de celdas de combustible a base de moléculas orgánicas pequeñas, como el ácido fórmico o el metanol.

PALABRAS CLAVES: Electrooxidación; Oscilaciones; Producción de entropía.

1. INTRODUCTION

A fundamental understanding of energy conversion and loss mechanisms is necessary to advance electrochemical cell technologies. This requires theoretical and experimental frameworks capable of capturing thermodynamic irreversibility. Recent research has focused on studying the efficiency limits of electrochemical systems. For instance, the integration of Solid Oxide Electrolyzers has demonstrated improved system-wide performance by leveraging high-temperature thermal energy (Saraf *et al.*, 2023). In solar-driven electrochemical platforms, particularly for CO_2 reduction to fuels, the thermodynamic limits on achievable efficiencies have been thoroughly analyzed (Chen *et al.*, 2020). Accurate modeling also depends on the characterization of temperature-dependent thermodynamic properties of electrochemical systems (Alahmed *et al.*, 2025). Similarly, Thermo-Electrochemical Cells designed to harvest low-grade waste heat have been evaluated using entropy-based assessments of energy-conversion performance (Fan *et al.*, 2022). Even in bio-electrochemical systems such as Microbial Fuel Cells, thermodynamic analyses play a role in optimizing bioelectricity generation and conversion efficiency from waste streams (Obileke *et al.*, 2021). These studies underscore the importance of incorporating precise thermodynamic information and entropy-based metrics into the modeling and design of electrochemical energy systems.

On the other hand, nonlinear dynamics provides a robust framework for understanding instabilities, bifurcations, and oscillations observed in electrochemical systems (Epstein *et al.*, 1998; Barragán, 2015a). In particular, oscillatory behavior during the electrooxidation of small organic molecules and the electrodissolution of metals has attracted considerable attention (Okamoto *et al.*, 1996; Delmonde *et al.*, 2016; Strasser, 2000). Studying such dynamics -and their dependence on physicochemical parameters- has shed light on the complex interplay among surface kinetics, charge transfer, and mass transport, which can give rise to electrochemical instabilities driven by positive and negative feedback loops.

Among these systems, the electrooxidation of small organic molecules such as formic acid and methanol is of particular interest due to its potential for low-emission fuel cells (Varela *et al.*, 2017). However, advancing these technologies requires a deeper understanding of the underlying reaction mechanisms, which often involve multiple parallel and sequential steps, adsorbed intermediates, nonlinear kinetics, and coupling with transport processes. In this context, relatively simple mathematical models are valuable tools: they capture the essential physicochemical characteristics of the system while enabling the exploration of electrochemical instabilities, oscillatory dynamics, and spatiotemporal patterns (Okamoto *et al.*, 1996; Mukouyama *et al.*, 2006; Perini *et al.*, 2020). The objective of this work is to evaluate the thermodynamic efficiency of a

simplified electrooxidation model by applying the Second Law of Thermodynamics to quantify the entropy generation under different dynamic regimes–steady state and sustained oscillations-induced by galvanostatic operation.

The model consists of a system of stiff ordinary differential equations derived from a proposed reaction scheme, coupled with mass, energy, and charge balances. While previous studies have focused primarily on mechanistic or dynamical aspects, here we emphasize the thermodynamic perspective. Traditional efficiency evaluations rely on the First Law, which compares energy input to energy output. However, the Second Law introduces a more refined view, based on quantifying entropy generation as a measure of irreversibility in processes such as chemical reactions, mass and heat transfer, and charge transport (Prigogine, 1961; De Groot *et al.*, 1984; Kondepudi, 2008). In this framework, entropy generation represents the energetic cost of irreversibility and provides insight into the internal dissipation mechanisms that limit system performance.

Electrochemical systems inherently operate under nonequilibrium conditions, driven by irreversible processes. In this study, we simulate a generic electrooxidation reaction under galvanostatic control and compute the entropy production associated with heat dissipation, charge transfer, and chemical reaction. Entropy generation is evaluated as a function of the applied current - used here as a control and bifurcation parameter - across both stationary and oscillatory regimes.

2. ELECTROCHEMICAL MODEL

The mathematical model employed in this work is derived from a reaction scheme originally proposed for the catalytic electrooxidation of formic acid (Okamoto *et al.*, 1996; Samjeské *et al.*, 2005; Perini *et al.*, 2020). These studies describe the dynamics of small organic molecules on platinum surfaces, highlighting the formation of adsorbed intermediates and their subsequent oxidation to carbon dioxide.

In this work, however, we adopt a more general formulation in which a generic small organic molecule S is electrooxidized to CO_2. This abstraction enables us to emphasize the fundamental structure of the reaction mechanism, which is common to the electrooxidation of various small organic molecules such as formic acid, methanol, acetaldehyde, and related compounds, without being constrained by the specific stoichiometry of a particular substrate. In particular, many of these systems share the same core sequence of steps: (i) reversible adsorption of the organic molecule onto the catalytic surface, (ii) formation of partially oxidized intermediates such as CO, and (iii) irreversible oxidation of those intermediates to CO_2.

The reaction scheme considered here includes two parallel pathways:
(A) S, maintained at constant concentration in the homogeneous phase, is electrochemically transformed at the electrode surface into an adsorbed intermediate, denoted as $\tilde{S}$, which occupies a fraction of the active sites. The adsorption of S is assumed to be a fast, reversible step. In contrast, the irreversible oxidation of

the adsorbed intermediate $\tilde{S}$ to carbon dioxide constitutes the rate-limiting surface reaction in this pathway.

(B) In the parallel route, S is dehydrated at the electrode surface to form adsorbed carbon monoxide, which also occupies active sites. Subsequently, the adsorbed CO is electrochemically oxidized to CO_2 via a surface reaction with water (Samjeské *et al.*, 2005).

The stoichiometry of each pathway depends on the molecular identity of S, which determines both the number of active sites involved in adsorption and the number of electrons transferred per reaction. Although we considered incorporating a variable stoichiometric coefficient to account for the structural diversity of different organic substrates, we decided to reserve this refinement for future work. Such extensions would require integrating additional kinetic models for adsorption and desorption, along with a more detailed characterization of S's molecular structure.

The purpose of the present model is to describe the dynamical response of the working electrode potential as a function of circuit parameters and interfacial processes (Bard *et al.*, 2001, pp 24-28). Accordingly, the minimum set of dynamic variables includes the applied current (under galvanostatic control), the electrode potential, and the fractional surface coverages of the adsorbed species $\tilde{S}$ and CO.

2.1. Equivalent electrical circuit

Figure 1 shows the electrical circuit representation of the three-electrode electrochemical cell operating under galvanostatic control (Bard *et al.*, 2001, pp 24-28). A galvanostat imposes a constant applied current J_{app}, which flows from the instrument to the counter electrode (CE). Since the CE carries the entire imposed current, its potential may drift significantly during operation. The working electrode (WE) is the site where the electrochemical reaction takes place. Its potential change is measured against the reference electrode (RE), which is ideally non-polarizable and draws no current. The RE is connected to a high-impedance voltmeter to monitor the WE potential without disturbing the electrochemical system. The diagram explicitly distinguishes two resistive contributions. The uncompensated resistance R_u represents the ohmic drop between the WE and the RE, which affects the measured potential. The element R_c denotes the dynamic interfacial response of the WE, including both faradaic kinetics and the capacitive behavior of the double layer. The CE-WE path through the electrolyte constitutes the overall cell resistance R_{cell}, which determines the potential required to sustain the imposed current. As the galvanostat maintains a constant current, the WE potential adjusts dynamically in response to interfacial reaction rates and ohmic losses in the cell. The equation describing the current density as a function of the overpotential during the electrochemical reaction at a working electrode can be written following the Butler-Volmer equation (Lefrou *et al.*, 2012):

$$I(t) = I_0 \left(\exp\left(\frac{\alpha n F}{RT} \eta(t) \right) - \exp\left(\frac{-(1-\alpha) n F}{RT} \eta(t) \right) \right) \tag{1}$$

Where:

- I_0: exchange current density.
- α: charge transfer coefficient.
- n: number of electrons involved in the redox reaction.
- F: Faraday's constant.
- R: gas constant.
- T: temperature in Kelvin.
- η: overpotential, the difference between the actual electrode and equilibrium potential.

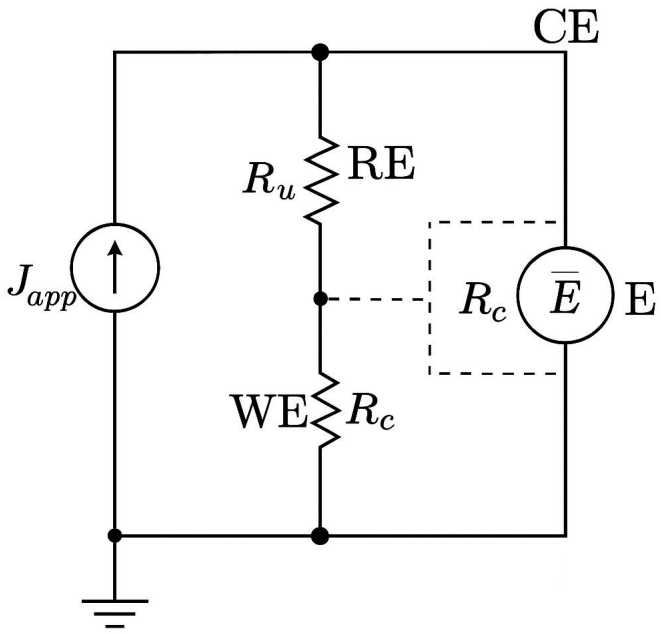

Figure 1: Schematic diagram of a three-electrode electrochemical cell under galvanostatic control. The working electrode (WE) potential is measured against the reference electrode (RE). The counter electrode (CE) completes the circuit, carrying the applied current J_{app}. The resistor R_u represents the uncompensated resistance between the RE and the WE. The resistor R_c represents the electrochemical interface. The potential $\overline{E}$ is the controlled variable, measured across the WE and RE; J_{app} acts as a control parameter for the operation and the dynamics of E. Source: Author's Own Work.

2.2. Kinetic equations

Following the description given at the beginning of this section, the electrochemical reactions governing the system are (Okamoto *et al.*, 1996):

$$S + 2* \rightleftharpoons \tilde{S} + e^- \tag{2}$$

$$\tilde{S} + * \rightarrow CO_2 + 3* + e^- \tag{3}$$

$$S + 2* \rightarrow CO + * \tag{4}$$

$$CO \rightarrow CO_2 + 2e^- + 3* \tag{5}$$

where * denotes surface active sites. The time evolution of the surface coverage fractions ($\theta_{\tilde{S}}$, θ_{CO}) and the electrode potential E are given by:

$$\frac{d\theta_{\tilde{S}}}{dt} = k_1^+ \theta_*^2 - k_1^- \theta_{\tilde{S}} - k_2 \theta_{\tilde{S}} \theta_* \tag{6}$$

$$\frac{d\theta_{CO}}{dt} = k_3 \theta_*^2 - k_4 \theta_{CO} \theta_* \tag{7}$$

$$C\frac{dE}{dt} = J_{\text{app}} - Fh\left(k_1^+ \theta_*^2 - k_1^- \theta_{\tilde{S}} + k_2 \theta_{\tilde{S}} \theta_* + 2k_4 \theta_{CO} \theta_*\right) \tag{8}$$

Where C is the double-layer capacitance, J_{app} is the applied external current density to the working electrode, h is the amount of surface site per unit area, n_i are the transferred electrons. The k_i are kinetic rate constants, and we assume that they can be expressed in terms of the Butler-Volmer equation, see Equation 1:

$$k = k_0 \exp\left(\frac{\alpha n F (E - E_{eq})}{RT}\right) \tag{9}$$

Where α_i is the charge transfer coefficient, and E_{eq} is the equilibrium potential.
From Equation (2) and Equation (4), the fraction of free active sites follows the next balance:

$$\theta_* = 1 - \theta_{CO} - 2\theta_{\tilde{S}} \tag{10}$$

2.2.1. Energy balance equation

To enhance the accuracy of the mathematical model regarding experimental conditions, we incorporated the energy balance equation to account for temperature control and its effects within the electrochemical cell. According to the First Law of Thermodynamics, the temperature change is determined by the balance between the enthalpy dissipated within the cell by the electrochemical process and the enthalpy transferred from the cell to the surrounding environment, specifically the thermostat. Then, the temperature, T, evolves as follows (Incropera, 1999; Sen *et al.*, 2008; Montoya *et al.*, 2021):

$$mC_p \frac{dT}{dt} = \sum_i V\left(-\Delta H_i - n_i F E\right) r_i - h_T A_r (T - T_{\text{ext}}) \tag{11}$$

Here, m is the total mass of the electrolyte (in grams), C_p is the specific heat capacity $[J/(gK)]$, and T is the reactor temperature. The term on the right-hand side represents the net rate of energy input and dissipation: the first term accounts for the heat released or absorbed by the chemical and electrochemical reactions, where ΔH_i is the enthalpy of reaction i, n_i is the number of electrons transferred, F is Faraday's constant, E is the electrode potential, r_i is the reaction rate $[mol/(Ls)]$, and V is the system volume $[L]$. The second term

accounts for heat loss to the surroundings by conduction, with h_T being the overall heat transfer coefficient $[W/(m^2-K)]$, A_r the reactor's surface area, and T_{ext} the external (thermostat) temperature. All terms in this expression are dimensionally consistent, with units of energy per unit time $[J/s]$.

In energy conversion processes such as electrochemical cells, the magnitude of the entropy generation rate serves as an indicator of efficiency loss compared to the maximum efficiency achievable under reversible conditions. Generally, a lower entropy generation rate corresponds to higher conversion efficiency. A direct application of entropy generation analysis is process optimization, which aims to identify irreversible steps with significant energy dissipation, such as those occurring during charge transport and heat transfer.

Previous studies have applied this thermodynamic framework to a variety of nonlinear dynamical systems. In the work of Villanueva *et al.* (2009), the entropy generation was calculated for a mechanical piston performing work due to an internal oscillatory chemical reaction. This analysis enabled the authors to evaluate the operating efficiency of a thermodynamic machine driven by chemical oscillations. In the study by Barragán *et al.* (2015b), entropy generation was analyzed in a heat-conduction calorimeter with an oscillatory reaction within the measurement cell. This approach enabled characterization of the energetic performance of both the reaction and the calorimetric device. More recently Montoya *et al.* (2024), applied entropy generation calculations to a complex reaction mechanism involving chemical oscillations, to identify kinetically significant steps responsible for irreversibility and to evaluate their energetic relevance.

In the present work, we incorporate into the mathematical model of the electrochemical process an estimate of entropy production arising from charge-transfer processes driven by overpotentials and from heat transport driven by temperature gradients. We also account for contributions from chemical reaction steps, thereby completing the thermodynamic characterization of the system.

The total entropy production rate is given by the sum of the contributions from chemical reactions, charge transport, and heat transport, as expressed in the following equation:

$$\sigma_{\text{total}} = \sigma_{\text{chem}} + \sigma_{\text{charge}} + \sigma_{\text{heat}}$$

Each of these thermodynamic quantities is described in the following sections.

2.3. Chemical reaction entropy production

Nonequilibrium thermodynamics postulates that thermodynamic forces arising from gradients in substances' chemical potentials drive reaction rates. We obtain the entropy production rate from the product of these forces and the corresponding flows, which is always a positive value (De Groot *et al.*, 1984; Kondepudi, 2008; Garrido, 2004). Therefore, the expression for the entropy generation rate for chemical reactions is:

$$\sigma_{\text{chem}} = -\frac{\sum r_i \Delta G_i}{T} \tag{12}$$

By considering only equations (3),(4), and (5), where electrochemical reactions occur, the expression for the rate of entropy production of the kinetic model is as follows:

$$\sigma_{\text{chem}} = -\frac{(k_2\theta_{\tilde{S}}\theta_*)\Delta G_2}{T} - \frac{(k_3\theta_{\tilde{S}}\theta_*^2)\Delta G_3}{T} - \frac{(k_4\theta_{CO}\theta_*)\Delta G_4}{T} \tag{13}$$

where ΔG_i are the Gibbs energy changes of the respective reactions, and T is the temperature.

2.4. Charge transfer entropy production

The overpotential drives the electric current density. Equations (2), (3), and (5) involve charge transfer, so the expression for calculating entropy generation is (De Groot *et al.*, 1984; Kondepudi, 2008; Garrido, 2004):

$$\sigma_{\text{charge}} = \frac{F}{T}[r_1\eta_1 + r_2\eta_2 + r_4\eta_4] \tag{14}$$

$$\sigma_{\text{charge}} = \frac{F}{T}[(k_1^+\theta_S\theta_*^2 - k_1^-\theta_{\tilde{S}})\eta_1 + (k_2\theta_{\tilde{S}}\theta_*)\eta_2 + (k_4\theta_{CO})\eta_4] \tag{15}$$

where $\eta_i = E - E_{\text{eq},i}$ is the overpotential.

2.5. Heat Transport Entropy Production

A temperature gradient leads to heat transport. Then, the entropy production rate is given by (De Groot *et al.*, 1984):

$$\sigma_{\text{heat}} = \frac{J_q}{T^2} \tag{16}$$

If we assume Newton's law expression for the heat flux, then the entropy production for heat transport is as follows:

$$\sigma_{\text{heat}} = \frac{h(T - T_{\text{ext}})}{T^2} \tag{17}$$

3. METHODOLOGY

It is worth noting that the present study adopts a macroscopic, system-level approach to entropy generation. The analysis does not include a decomposition of the entropy generated into fractions absorbed or retained by individual chemical species or interfacial phases. Instead, the entropy production terms associated with charge transfer, heat transport, and chemical reactions are computed globally and interpreted as measures of internal dissipation.

The numerical solution of the system of ordinary differential equations, equations (6),(7), (8), and (11), was performed using MATLAB *R*2019*a* software with the `ode15s` solver and a tolerance of 10^{-10}. The solution values were used to compute equations (16) and (18).

In this study, we do not calculate equation (14) because the entropy generation of a chemical reaction is a characteristic property that cannot be optimized within the established reaction mechanism. This value becomes significant when comparing reactions or when simplifying a reaction mechanism by eliminating steps that generate minimal entropy. Additionally, the entropy generation rate from chemical reactions is several orders of magnitude higher than that from transport processes. However, the qualitative behavior of this quantity is similar to that of transport processes.

Some of the parameters used for the simulation are (Roelofs, 1988; Klotz *et al.*, 2008; Lefrou *et al.*, 2012): Faraday constant, $F = 96500\ C/mol$; gas constant, $R = 8.314\ J/(molK)$; Thermostat temperature, $T_{ext} = 298.15\ K$; Volume of a cylindrical glass reactor, $V = 50\ mL$; Reactor hight, $h_r = 6\ cm$; Density of liquid phase, $\rho = 1{,}010\ g/mL$; Heat capacity of liquid phase, $C_p = 4.184\ J/(gK)$; Global heat transfer coefficient of the reactor, $h_T = 100\ W/m^2K$; Charge transfer coefficient, $\alpha = 0.5$; Internal resistance of the electrolyte, $R_{int} = 10\ Ohm$; Density of active sites, $h = 2.2 \times 10^{-9}\ mol/cm^2$; Electrode area, $A = 1\,cm^2$, and Electrochemical equilibrium potentials: $E_{eq,1} = 25\ mV$, $E_{eq,1_{rev}} = 25\ mV$, $E_{eq,2} = 5\ mV$, $E_{eq,3} = 0.01\ mV$, $E_{eq,4} = 55\ mV$. Capacitance of the double layer can range between $C = 2 \times 10^{-5}\ F/cm^2$ and $C = 8 \times 10^{-5}\ F/cm^2$ (Merlet *et al.*, 2022). The initial adsorbed fraction of the chemical species was set to 0.1.

4. RESULTS AND ANALYSIS

Based on the simulations, we determined that the external current applied through a galvanostat is the only parameter capable of modeling the oscillatory dynamics and the transition from steady to oscillatory states. The mathematical model is also sensitive to variations in the kinetic constants and equilibrium electrochemical potentials; specifically, changes greater than $5mV$ in the equilibrium potentials can keep the system stable or prevent the model from converging to a solution. Under the parameter values described in the methodology section, we observed oscillations in all variables of the mathematical model, including adsorbed chemical species, electrode potential, temperature, and entropy generation rates. Additionally, the reactor's overall heat-transfer coefficient ensures negligible temperature changes, indicating that the thermostat's thermal control is functioning correctly in the model.

4.1. Kinetic modeling

Although the applied current remains constant in all simulations, we acknowledge that the total charge transferred, $Q(t) = J_{\text{app}} \cdot t$, constitutes an physically meaningful measure of the extent of electrochemical reaction. Representing system variables as functions of Q-rather than time-can be especially useful when the current varies or when comparing systems under different dynamic constraints. However, under the galvanostatic conditions employed in this work, time and charge are linearly related. Therefore, the qualitative behavior of key variables (such as $\tilde{S}$, CO surface coverages, electrode potential, and temperature) remains unchanged whether plotted as functions of time or charge. For this reason, we report the system dynamics in the time domain only, noting that the underlying results apply equally well when expressed in terms of

charge transferred.

In Figure 2, we see how the temporal dynamics of the adsorbed fraction of the active species, $\tilde{S}$, change with the magnitude of the applied external current. The adsorbed fraction increases with higher external current, rising from 0.1 at low current (lower blue line) to 0.27 at 0.30 mA/m^2 (upper red line). Notably, the applied external current serves as both a control parameter and a bifurcation parameter. As the current magnitude increases, the system transitions from steady states to limit-cycle oscillations, passing through a phase of damped oscillations.

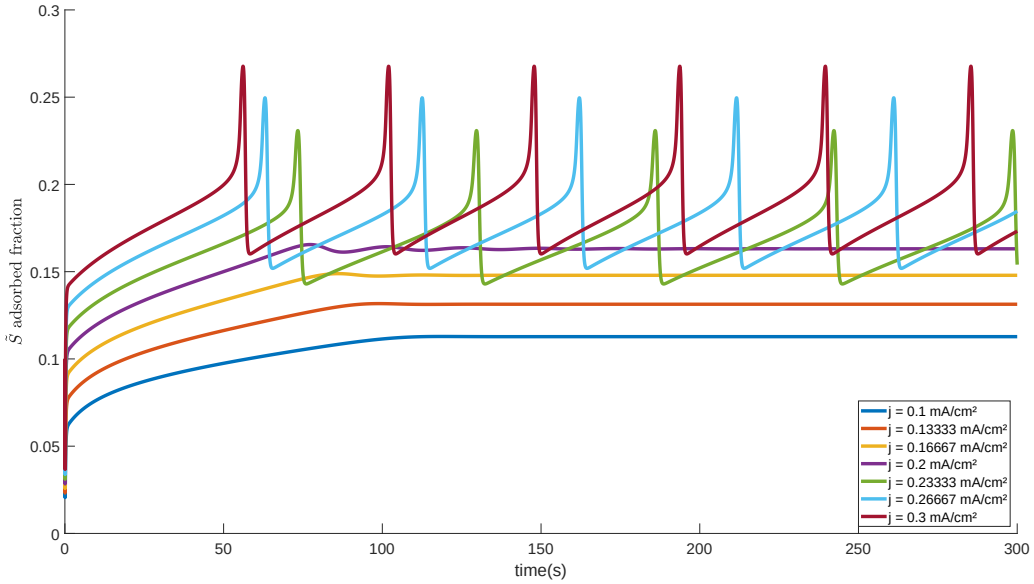

Figure 2: Time evolution of the adsorbed fraction of $\tilde{S}$ for different values of the parameter J_{app}, from 0.1 mA/cm^2 to 0.3 mA/cm^2. Source: Author's Own Work.

Figure 3 shows how the temporal dynamics of the adsorbed fraction of carbon monoxide change with the magnitude of the applied external current. In contrast to what is observed in Figure 3, the adsorbed carbon monoxide CO fraction decreases as the applied external current increases.

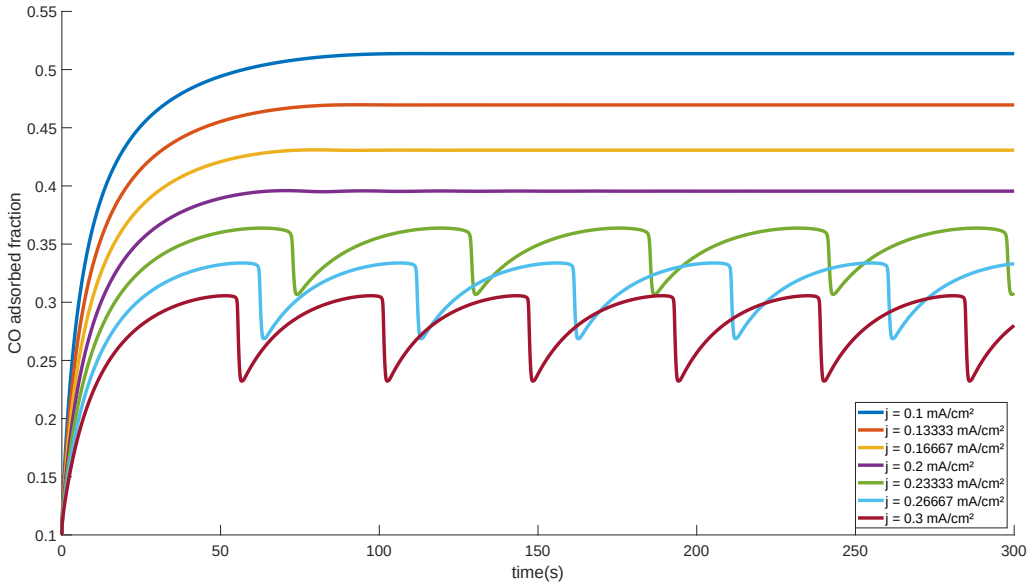

Figure 3: Time evolution of the adsorbed fraction of CO for different values of the parameter J_{app}, from 0.1 mA/cm^2 to 0.3 mA/cm^2. Source: Author's Own Work.

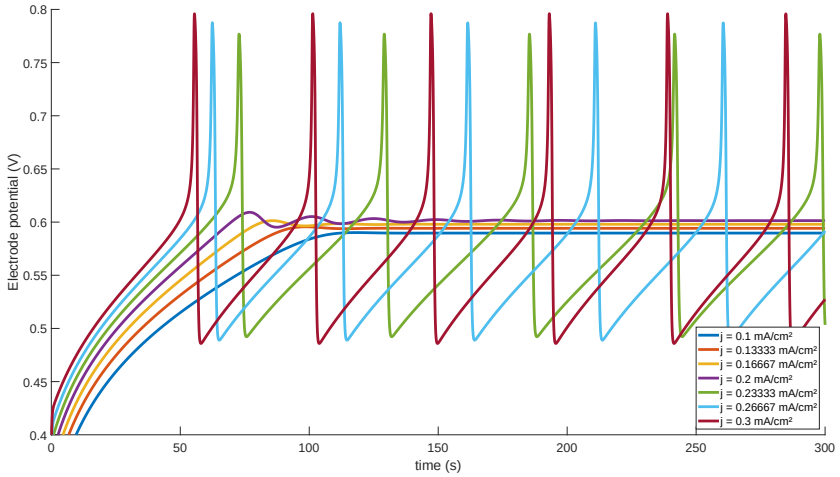

Figure 4: Time evolution of the electrode potential for different values of the parameter J_{app}, from 0.1 mA/cm^2 to 0.3 mA/cm^2. Source: Author's Own Work.

This behavior indicates that the transition from a steady state to a limit cycle occurs as the CO coverage on the electrode surface diminishes. Notably, at low currents, the adsorbed fraction of CO occupies approximately 50 % of the active sites. Several researchers have highlighted the role of CO in generating electrochemical instabilities during the electrooxidation of certain organic substances.

To the working electrode potential, Figure 4 shows that the potential dynamics consistently reach up to $\sim$ 60 mV across the range of external currents applied to the circuit, which varies from 0.1 mA/cm^2 to 0.30

mA/cm^2. The potential remains steady at low applied external currents, whereas at higher currents it exhibits oscillatory behavior. Although the amplitude of these oscillations exceeds 30 mV, the average value of the oscillating potential consistently remains close to ~ 60 mV.

The above results align with existing knowledge about this electrochemical system. The signal recorded at the working electrode indicates the specific electrochemical process that is occurring. When an external current is applied, it affects the adsorption of specific chemical species, such as carbon monoxide (CO), thereby causing fluctuations in the electrochemical cell's potential.

Before conducting the Second Law thermodynamic evaluation of the dynamics of the mathematical model, it is essential to account for the effect of temperature on the kinetic constants and the electrode potential. This consideration is important because heat-transfer losses can be substantial. To minimize temperature fluctuations within the cell, we employed an overall heat-transfer coefficient of 100 $W/(m^2K)$, which can be achieved with a thermostat and a glass cell. As shown in Figure 5, the temperature change does not exceed 0.1 K, even under the highest applied external current. Notably, the oscillatory dynamics require the largest temperature variation relative to the thermostat temperature.

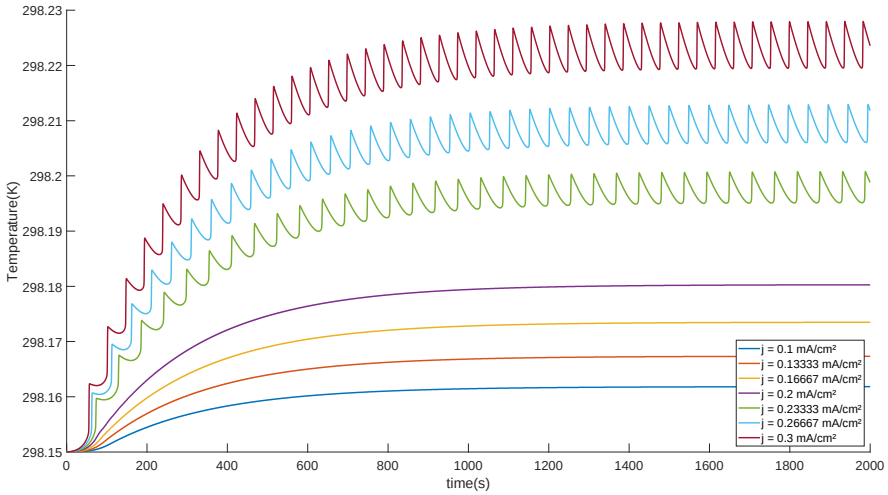

Figure 5: Time evolution of the reactor temperature for different values of the parameter J_{app}, from 0.1 mA/cm^2 to 0.3 mA/cm^2. Source: Author's Own Work.

4.2. Entropy production rate

Similarly, as shown in Figure 5, the entropy generation rates follow the dynamics of the electrochemical process described by the mathematical model. Figure 6 illustrates how entropy generation associated with oscillatory dynamics guides the system to a specific region of the phase plane, forming a limit-cycle attractor. The size of this attractor in the state space determines the Second Law energy efficiency of the electrochemical transport process.

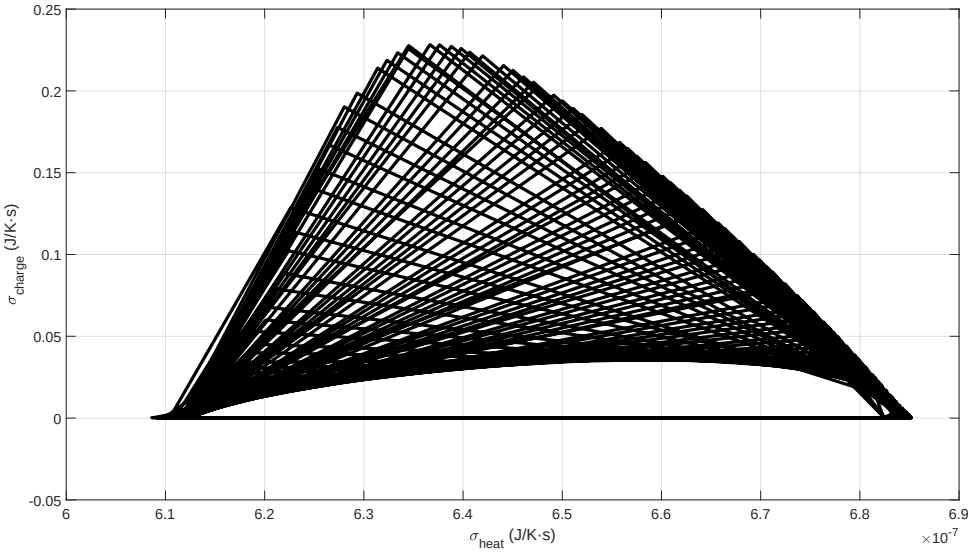

Figure 6: Limit cycle attractor in the phase diagram of entropy production rates. The control parameter J_{app} was set to $0.3 mA/cm^2$. Source: Author's Own Work.

To quantify the entropy generation rate as a function of the control parameter (the applied current), we compute the time-averaged entropy production by integrating over a sufficiently long interval to ensure that the system either reaches a steady state or exhibits sustained oscillations, as defined in Equation 18. A total integration time of 2000 seconds is used, as shown in Figure 5. The results are presented in Figures 7, 8, and 9.

Two key observations arise from this analysis. First, the average entropy generation due to heat transport is negligible-several orders of magnitude lower than that associated with charge transfer- and both contributions are, in turn, significantly smaller than the entropy production associated with chemical reactions. Second, a qualitative change in entropy generation is observed at the bifurcation point, marking the onset of sustained oscillations. This transition reflects a shift in the system's dynamical behavior and suggests that average entropy generation may serve as an indicator of the regime.

Furthermore, the emergence of a limit cycle, representing sustained oscillatory behavior, is accompanied by a marked increase in entropy generation. In accordance with the Second Law of Thermodynamics, this increase implies a reduction in thermodynamic efficiency, reinforcing the idea that dynamic complexity entails greater irreversibility.

$$\langle \sigma \rangle = \frac{1}{t} \int_0^t \sigma(t)\, dt \tag{18}$$

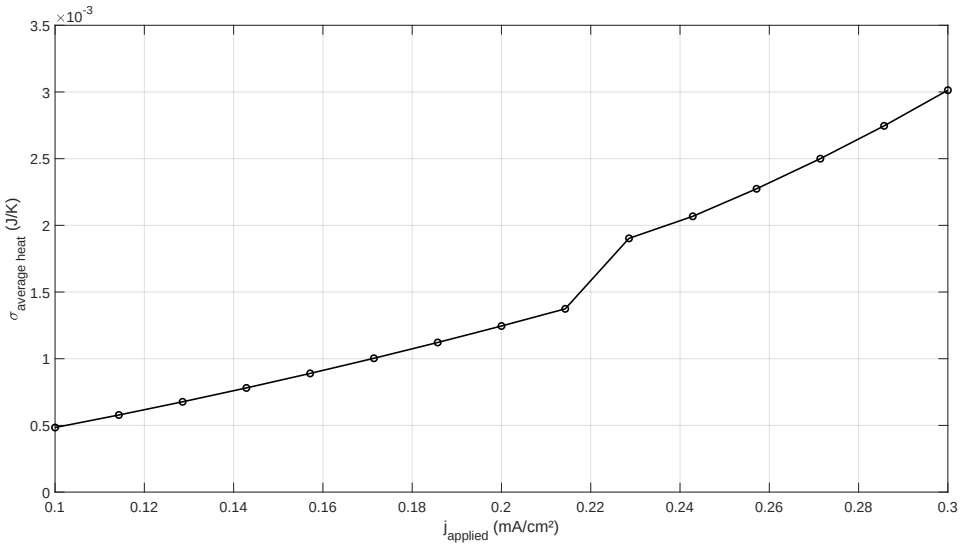

Figure 7: Average heat transport entropy production as a function of the control parameter J_{app}. The average is calculated over an integration time of 2000 seconds. Source: Author's Own Work.

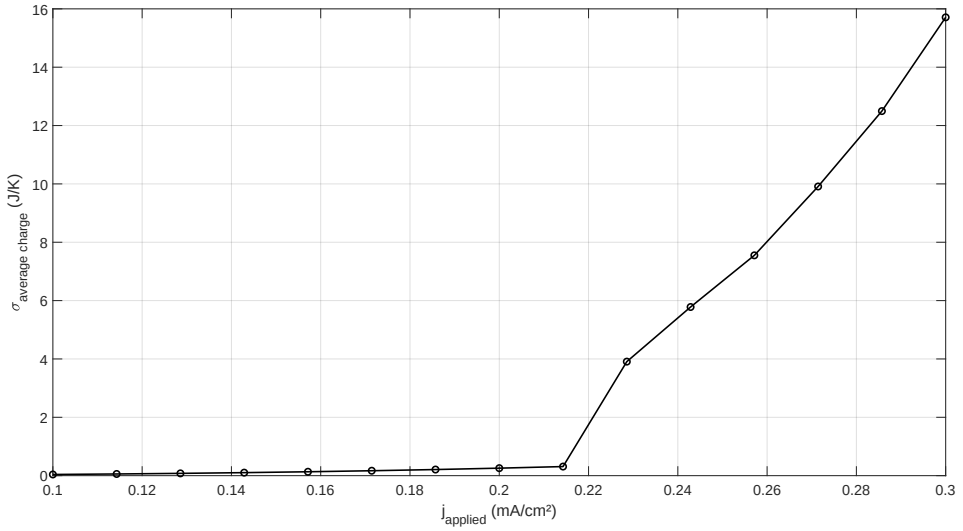

Figure 8: Average charge transfer entropy production as a function of the control parameter J_{app}. The average is calculated over an integration time of 2000 seconds. Source: Author's Own Work.

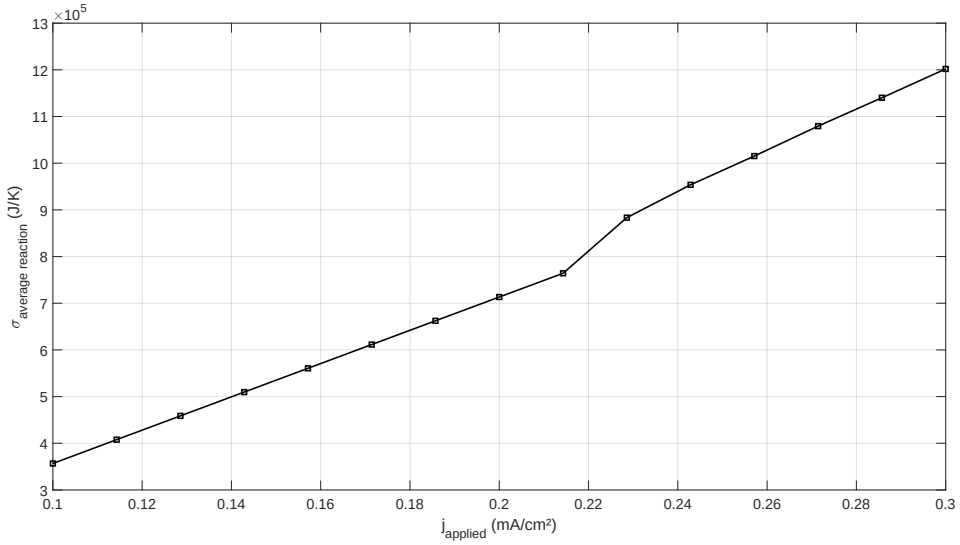

Figure 9: Average chemical reaction entropy production as a function of the control parameter J_{app}. To compute equations (12) and (13), we assume the following values for Gibbs energy changes: $\Delta G_2 = -80kJ/mol$; $\Delta G_3 = +20kJ/mol$; $\Delta G_4 = -120kJ/mol$. The average is calculated over an integration time of 2000 seconds. Source: Author's Own Work.

The inclusion of chemical reaction entropy production, Equation 12, (Figure 9), provides a more complete thermodynamic description of the system's irreversibility. Unlike contributions from heat and charge transport, which are predominantly influenced by thermal boundary conditions and circuit resistance, the entropy generated by the reaction pathway directly reflects the internal energy dissipated during molecular transformations at the electrode surface. As observed in Figure 9, this contribution is dominant across all values of the control parameter J_{app} and exhibits an apparent increase at the bifurcation point. This indicates that a greater rate of chemical energy dissipation supports the transition to sustained oscillations.

From a mechanistic perspective, the entropy generated by the irreversible transformation of the adsorbed species $\tilde{S}$ into CO_2, along with the dehydration pathway leading to CO formation, contributes significantly to the overall entropy budget. These processes involve breaking and forming chemical bonds under electrochemical control and constitute the core of the energy-conversion mechanism. Therefore, the entropy production rate from the chemical reaction not only dominates the total entropy generation but also captures the intrinsic irreversibility of the electrooxidation process.

Overall, the addition of this chemical reaction contribution strengthens the thermodynamic analysis and reinforces the interpretation of average entropy generation as a reliable descriptor of the system's dynamic and energetic behavior, particularly near bifurcation points and in regimes of sustained nonlinear oscillations.

These results have practical relevance for optimizing electrochemical energy systems, particularly fuel cells based on the electrooxidation of small organic molecules. The emergence of oscillatory regimes-driven by feedback between surface coverage and reaction kinetics- is accompanied by a marked increase in entropy

generation, as quantified in this study. This increase reflects higher internal dissipation and, consequently, a reduction in energy-conversion efficiency in accordance with the Second Law of Thermodynamics. Therefore, identifying operating conditions that suppress or delay the onset of oscillations, or minimize entropy per unit charge transferred, is essential for improving the overall performance and durability of fuel cell systems.

5. CONCLUSIONS

Starting from a simplified yet representative reaction scheme, we developed a mathematical model that captures the essential dynamic behavior of an electrooxidation process under galvanostatic control. The model reproduces both steady-state and sustained oscillatory regimes as the applied current density is varied, consistent with well-known features of nonlinear electrochemical systems.

A central contribution of this work is the thermodynamic evaluation of these regimes based on entropy generation. By explicitly quantifying the entropy production associated with heat transfer, charge transport, and chemical reactions, we demonstrated that a distinct average entropy generation rate characterizes each dynamic state. Notably, the transition from steady-state to oscillatory dynamics at the bifurcation point is accompanied by a sharp increase in entropy production, reflecting a higher energetic cost and a reduction in thermodynamic efficiency as predicted by the Second Law.

Although this study represents an initial exploration, it highlights the value of integrating nonlinear dynamics with nonequilibrium thermodynamics to assess the internal dissipation and efficiency of electrochemical systems. This approach provides a foundation for further investigations into entropy-based optimization strategies for energy conversion devices, such as fuel cells.

Declaration of conflicts of interest

The authors declare no conflict of interest

Acknowledgment

We thank the Faculty of Sciences of the Universidad Nacional de Colombia, Medellín campus, for partially funding this work through the Academic Teaching Program Research Project HERMES-58375.

Author's contributions

Carolina Cáceres-Molano contributed to the formulation of the research problem, the description of the mathematical model, the analysis of the results, and the writing of the first draft of the manuscript.

Daniel Barragán contributed to the formulation of the research problem, the description of the model, the programming of the computational simulations, the analysis of the results, and the preparation of the manuscript.

References

Alahmed, A., Kucukoglu, O., Kucukoglu, N., & Isgor, O. B. (2025). Measuring Temperature-Dependent Thermodynamics of Electrochemical Reactions. *ACS Measurement Science Au*, **5(1)**, 1–7.

Bard, A. J., & Faulkner, L. R. (2001). Electrochemical methods: fundamentals and applications. Second edition. John Wiley & Sons.

Barragán, D. (2015). Essentials of kinetics and thermodynamics for understanding chemical oscillations. *Foundations of Chemistry*, 17(**2**), 93–106.

Barragán, D., Ágreda, J., & Parra, W. (2015). Entropy production in the Oregonator model perturbed in a calorimeter with a chemical pulse. *Journal of Thermal Analysis and Calorimetry*, 119(**1**), 705-713.

Chen, S., Li, Y., & Lewis, N. S. (2020). Thermodynamic and achievable efficiencies for solar-driven electrochemical reduction of carbon dioxide to transportation fuels. *Proceedings of the National Academy of Sciences*, 117(**23**), 12711–12718.

De Groot, S. R., & Mazur, P. (1984). Non-equilibrium thermodynamics. New York:Dover.

Delmonde, M. V. F., Sallum, L. F., Perini, N., Gonzalez, E. R., Schlogl, R., & Varela, H. (2016). Electrocatalytic efficiency of the oxidation of small organic molecules under oscillatory regime. *The Journal of Physical Chemistry C*, 120(**39**), 22365–22374.

Epstein, I. R., & Pojman, J. A. (1998). An introduction to nonlinear chemical dynamics: oscillations, waves, patterns, and chaos. Oxford University Press.

Fan, L., Zhai, D., Wang, Y., Zhang, W., & Chen, J. (2022). Advances in Thermo-Electrochemical (TEC) Cell Performances for Harvesting Low-Grade Heat Energy: A Review. *Sustainability*, 14(**15**), 9483.

Garrido, J. (2004). Thermodynamics of electrochemical systems. *The Journal of Physical Chemistry B*, 108(**47**), 18336–18340.

Incropera, Frank P. (1999). Fundamentos de transferencia de calor. Cuarta edición. Prentice Hall.

Kikuchi, M., Miyahara, S., Mukouyama, Y., & Okamoto, H. (2008). Potential oscillation generated by formic acid oxidation in the presence of dissolved oxygen. *The Journal of Physical Chemistry C*, 112(**18**), 7186–7192.

Klotz, I. M. & Rosenberg, R. M. (2008) Chemical Thermodynamics: Basic concepts and methods. Seventh Edition. Wiley-Interscience.

Kondepudi, D. (2008). Introduction to modern thermodynamics. Wiley.

Lefrou, C., Fabry, P., & Poignet, J. C. (2012). Electrochemistry: the basics, with examples. Springer Science and Business Media.

Merlet, C., & Simon, P. (2022). Microscopic simulations of electrochemical double-layer capacitors. *Chemical reviews*, 122(**12**), 10837–10878.

Montoya, J. P., & Barragán, D. (2021). Producción de entropía en un modelo autocatalítico no-isotérmico perturbado con pulsos de analito. *Revista de la Facultad de Ciencias*, 10(**2**), 9–27.

Montoya, J. P., Peyares, A. C., & Barragán, D. (2024). The formalism of chemical thermodynamics applied to an oscillatory multistep chemical system. *Ingeniería e Investigación*, 44(**2**), 1.

Mukouyama, Y., Kikuchi, M., Samjeské, G., Osawa, M., & Okamoto, H. (2006). Potential oscillations in galvanostatic electrooxidation of formic acid on platinum: A mathematical modeling and simulation. *The Journal of Physical Chemistry B*, 110(**24**), 11912–11917.

Naito, M., Okamoto, H., & Tanaka, N. (2000). Dynamics of potential oscillations in the electrochemical oxidation of formic acid on Pt. *Physical Chemistry Chemical Physics*, 2(**6**), 1193–1198.

Obileke, K., Onyeaka, H., Meyer, E. L., & Nwokolo, N. (2021). Microbial fuel cells, a renewable energy technology for bio-electricity generation: A mini-review. *Electrochemistry Communications*, 125, 107003.

Okamoto, H., Tanaka, N., & Naito, M. (1996). Modelling temporal kinetic oscillations for electrochemical oxidation of formic acid on Pt. *Chemical physics letters*, 248(**3-4**), 289–295.

Perini, N., Delmonde, M. V., Ranjan, C., & Varela, H. (2020). Mechanistic aspects of the comparative oscillatory electrochemical oxidation of formic acid and methanol on platinum electrode. *Journal of Solid State Electrochemistry*, 24, 1811–1818.

Prigogine, I.(1961). Introduction to thermodynamics of irreversible processes. New York: Interscience Publishers.

Roelofs, M. G. (1988). Heat production in steady states and oscillations. *The Journal of chemical physics*, 88(**9**), 5516–5524.

Samjeské, G., Miki, A., Ye, S., Yamakata, A., Mukouyama, Y., Okamoto, H., & Osawa, M. (2005). Potential oscillations in galvanostatic electrooxidation of formic acid on platinum: A time-resolved surface-enhanced infrared study. *The Journal of Physical Chemistry B*, 109(**49**), 23509–23516.

Saraf, L. M., Senthil Kumar, N., & Chandramohan, V. P. (2023). Solid Oxide Electrolyzers Process Integration: A Comprehensive Review. *Applied Sciences*, 13(**8**), 4966.

Sen, S., Riaz, S. S., & Ray, D. S. (2008). Temperature dependence and temperature compensation of kinetics of chemical oscillations; Belousov-Zhabotinskii reaction, glycolysis and circadian rhythms. *Journal of theoretical biology*, 250(**1**), 103-112.

Strasser, P. (2000). Electrochemistry in self-organized dynamical states: Current oscillations and potential patterns in electrocatalytic reactions. *The Electrochemical Society Interface*, 9(**4**), 46.

Varela, H., Delmonde, M. V., & Zülke, A. A. (2017). The oscillatory electrooxidation of small organic molecules. Electrocatalysts for Low Temperature Fuel Cells: Fundamentals and Recent Trends, 145-163.

Villanueva-Marroquín, J., & Barragán, D. (2009). Análisis de la producción de entropía en una máquina térmica operada con un sistema químico no-lineal. *Revista mexicana de ingeniería química*, 8(**1**), 145–152.